JPEDAV (2012) 33:293–302
DOI: 10.1007/s11669-012-0048-6
1547-7037 ©ASM International

Gibbs Energy of Formation of $Ca_3Ti_8Al_{12}O_{37}$ and Phase Relations and Chemical Potentials in the System Al_2O_3-TiO_2-CaO

K. T. Jacob and G. Rajitha

(Submitted July 5, 2011; in revised form October 25, 2011)

The quaternary oxide in the system Al_2O_3-CaO-TiO_2 is found to have the composition $Ca_3Ti_8Al_{12}O_{37}$ rather than $CaTi_3Al_8O_{19}$ as reported in the literature. The standard Gibbs energy of formation of $Ca_3Ti_8Al_{12}O_{37}$ from component binary oxides is measured in the temperature range from 900 to 1250 K using a solid-state electrochemical cell incorporating single crystal CaF_2 as the solid electrolyte. The results can be represented by the equation:

$$\Delta G^{o}_{f(ox)}(\pm 70)/\mathrm{J\,mol^{-1}} = -248474 - 15.706(T/\mathrm{K}).$$

Combining this information with thermodynamic data on calcium aluminates and titanates available in the literature, subsolidus phase relations in the pseudo-ternary system Al_2O_3-CaO-TiO_2 are computed and presented as isothermal sections. The evolution of phase relations with temperature is highlighted. Chemical potential diagrams are computed at 1200 K, showing the stability domains of the various phases in the chemical potential-composition space. In each chemical potential diagram, chemical potential of one component is plotted against the cationic fraction of the other two components. The diagrams are valid at relatively high oxygen potentials where Ti is present in its four-valent state in all the oxide phases.

Keywords $Ca_3Ti_8Al_{12}O_{37}$, chemical potential diagram, enthalpy of formation, entropy, free energy of formation, isothemal section, phase diagram, system Al_2O_3-TiO_2-CaO

1. Introduction

Complex oxides in the system Al_2O_3-TiO_2-CaO are of potential use in nuclear waste containment. Morgan[1] tried to synthesize the inter-oxide compound $CaTi_3Al_8O_{19}$, which is isotypic with $SrTi_3Al_8O_{19}$,[2] using several methods. The most successful synthetic strategy involved co-precipitation and subsequent heating at a slow rate of 0.005 K s^{-1} to 1623 K after holding at 873 K for 86 ks. Even under the optimum synthetic conditions, pure $CaTi_3Al_8O_{19}$ was not obtained; small amounts of secondary phases such as Al_2O_3, $CaAl_{12}O_{19}$, and TiO_2 were always present. Morgan[1] did not analyze the composition of the complex oxide but relied on information from an unpublished report of Kesson and Ringwood, cited as reference 2 in their article.

K. T. Jacob, and **G. Rajitha,** Department of Materials Engineering, Indian Institute of Science, Bangalore 560012, India. Contact e-mail: katob@materials.iisc.ernet.in.

Partial isothermal sections of the phase diagram for the system Al_2O_3-TiO_2-CaO ($X_{CaO} \le 0.5$) in air were developed by Morgan and Koutsoutis[3] in the temperature range from 1273 to 1693 K. Two sections were presented, one valid from 1273 to 1628 K and the other from 1628 to 1693 K. The presence of Al_2TiO_5 as a stable phase along the Al_2O_3-TiO_2 binary above 1628 K is the essential difference between the two isothermal sections. These figures are also reproduced in the AcerS-NIST compilation of phase equilibrium diagrams for ceramic systems.[4,5] Other than several aluminate and titanate phases along the binary edges, only one complex oxide $CaTi_3Al_8O_{19}$ was detected inside the ternary triangle. Tie-lines connect $CaTi_3Al_8O_{19}$ to $CaTiO_3$, TiO_2 and Al_2O_3. $CaTi_3Al_8O_{19}$ coexists with Al_2O_3 and TiO_2 between 1273 and 1628 K. Above 1693 K, $CaTi_3Al_8O_{19}$ is unstable.

Since there is no thermodynamic data on $CaTi_3Al_8O_{19}$ reported in the literature, an attempt was made to measure its standard Gibbs energy of formation as a function of temperature using a solid-state cell based on single crystal CaF_2 as the electrolyte. During the course of the investigation it was found that the composition of the complex oxide reported in the literature is incorrect. The actual compound formed inside the ternary triangle has the composition $Ca_3Ti_8Al_{12}O_{37}$ with monoclinic unit cell (space group C^*/c, $Z = 8$) almost identical to that ascribed earlier to $CaTi_3Al_8O_{19}$.[1] Thermodynamic properties of $Ca_3Ti_8Al_{12}O_{37}$ were then measured. From the thermodynamic data, subsolidus phase relations in the system Al_2O_3-TiO_2-CaO were calculated at high oxygen chemical potentials corresponding to the presence of titanium in four-valent (Ti^{4+}) state.

2. Experimental Methods

2.1 Materials

The starting materials were $CaCO_3$, TiO_2 (rutile type), and α-Al_2O_3 of mass fraction purity >0.9999. Initially attempts were made to synthesize $CaTi_3Al_8O_{19}$ in air using the optimized heat-treatment procedure recommended by Morgan.[1] However, significant quantities of Al_2O_3 or $CaAl_{12}O_{19} + TiO_2$ were always present along with the complex oxide. A careful examination of the composition of the complex oxide using EDS and EPMA suggested a composition close to $Ca_3Ti_8Al_{12}O_{37}$. The composition is based on the ratio of Ca:Ti:Al in the quaternary oxide obtained using EPMA and assuming that titanium is present in four-valent state. Within experimental uncertainty, the cationic ratio in the quaternary oxide was almost the same in the single phase and three-phase samples. Results of composition analysis of the quaternary oxide in different phase fields are presented in Table 1.

As seen from Fig. 1, attempts to synthesize $CaTi_3Al_8O_{19}$ will result in a phase mixture of $Ca_3Ti_8Al_{12}O_{37} + Al_2O_3$, or $Ca_3Ti_8Al_{12}O_{37} + CaAl_{12}O_{19} + TiO_2$ if $CaAl_{12}O_{19}$ formed as an intermediate phase during synthesis and continued to exist as a metastable phase. Attempts were then made to make the new composition by heating mixtures of CaO, TiO_2, and Al_2O_3 in the appropriate molar ratio contained in platinum crucibles at 1623 K for a total of ~350 ks in dry air with two intermediate grinding and repelletization. A reactive form of CaO, obtained by decomposition of $CaCO_3$ in vacuum ($p \approx 10$ Pa) at 1100 K, was used in the preparation of the quaternary oxide. The other two oxides, TiO_2 and Al_2O_3, were dried at 573 K before use. The mixtures of component oxides were pelletized at a pressure of 100 MPa using a steel die before heating. Progress of reaction was followed by powder x-ray diffraction (XRD) analysis of the product. Single phase $Ca_3Ti_8Al_{12}O_{37}$ was obtained after a long heat treatment. The XRD pattern obtained in this study for $Ca_3Ti_8Al_{12}O_{37}$ is compared with that reported by Morgan[1] for $CaTi_3Al_8O_{19}$ in Fig. 2. The patterns are almost identical. Morgan[1] recorded the diffraction pattern only for $2\theta < 35°$. $Ca_3Ti_8Al_{12}O_{37}$ has monoclinic structure with cell parameters $a = 2.262$ nm, $b = 1.105$ nm, $c = 0.9752$ nm, and $\beta = 98.86°$, close to values suggested by Morgan[1] for the unit cell of $CaTi_3Al_8O_{19}$. The synthetic difficulties encountered by Morgan,[1] at least in part, appear to arise from the assumption of a wrong composition for the quaternary oxide. The correct composition of the quaternary oxide is $Ca_3Ti_8Al_{12}O_{37}$. Preliminary experiments indicated that this compound can coexist at equilibrium with Al_2O_3 and TiO_2.

Transparent single crystals of CaF_2 for use as solid electrolytes were obtained in the form of disks, 1.5 cm in diameter and 0.3 cm thick. The high-purity oxygen gas,

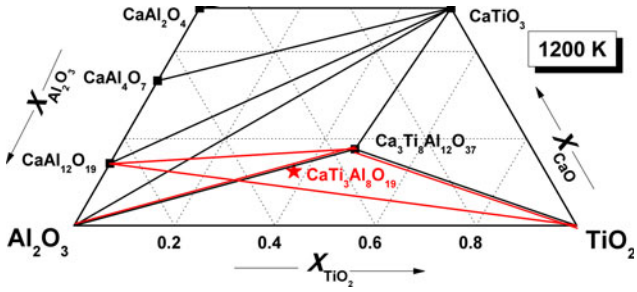

Fig. 1 Partial isothermal section of the phase diagram of the system Al_2O_3-TiO_2-CaO, demonstrating possible outcomes of attempts to synthesize $CaTi_3Al_8O_{19}$

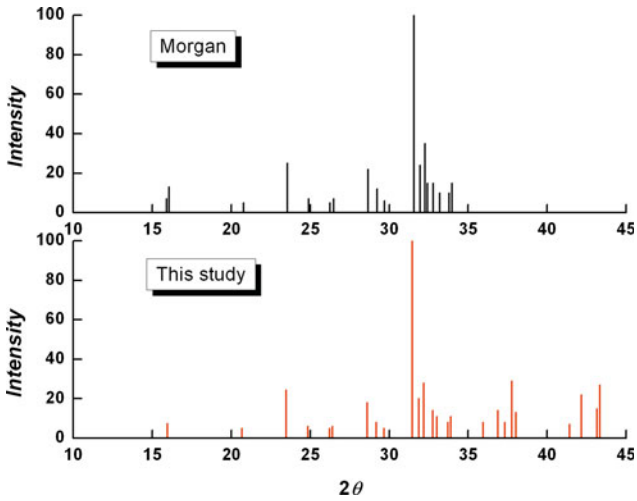

Fig. 2 Comparison of the XRD pattern for the compound $Ca_3Ti_8Al_{12}O_{37}$ obtained in this study with that reported by Morgan[1] for $CaTi_3Al_8O_{19}$

Table 1 Composition of the quaternary oxide in different phase fields of the system Ca-Ti-Al-O from EPMA

Serial number	Nominal composition	Phases identified by XRD/SEM/EDS	Average composition of quaternary oxide from EPMA Ca:Ti:Al atom ratio
1	$CaTi_3Al_8O_{19}$	$Ca_3Ti_8Al_{12}O_{37} + Al_2O_3 + TiO_2$ (trace)	1:2.660:4.010 (3:7.98:12.03)
2	$CaTi_3Al_8O_{19}$	$Ca_3Ti_8Al_{12}O_{37} + CaAl_{12}O_{19} + TiO_2$	1:2.657:4.013 (3:7.97:12.04)
3	$Ca_3Ti_8Al_{12}O_{37}$	$Ca_3Ti_8Al_{12}O_{37}$ (pure phase)	1:2.673:4.007 (3:8.02:12.02)
4	$X_{CaO} = 0.2$ $X_{TiO_2} = 0.6$ $X_{Al_2O_3} = 0.2$	$Ca_3Ti_8Al_{12}O_{37} + CaTiO_3 + TiO_2$	1:2.677:3.993 (3:8.03:11.98)

used to fix the oxygen potential over the electrodes of the solid-state cell, was passed through sodium hydroxide to remove traces of CO_2 and then dried by passing through columns containing anhydrous magnesium perchlorate and phosphorus pentoxide.

2.2 Apparatus and Procedure

The reversible emf of the solid-state cell,

$$O_2/Au,\ CaO + CaF_2//CaF_2//CaF_2 + Al_2O_3 + TiO_2 + Ca_3Ti_8Al_{12}O_{37},\ Au/O_2 \quad \text{(Eq 1)}$$

was measured as a function of temperature in the range from 900 to 1250 K. The cell is written such that the right-hand electrode is positive. The reference electrode consisted of an intimate equimolar mixture of CaO and CaF_2. The mixture was pelletized at 100 MPa and sintered in a stream of pre-purified oxygen at 1250 K. The measuring electrode, consisting of an equimolar mixture of four phases CaF_2, Al_2O_3, TiO_2, and $Ca_3Ti_8Al_{12}O_{37}$, was also pelletized and sintered under identical conditions. The particle size of the powders used to make the electrodes was in the range 3-12 μm. The use of nanosize particles was avoided since it can affect measured emf.[6] Minor variation in the mixing ratio of the constituents forming the electrode did not affect the cell emf. The presence of CaF_2 in the electrode pellets was found necessary to generate fluorine chemical potentials at the electrodes. Since fluorine ions are the mobile species in the CaF_2 solid electrolyte, the cells respond to the difference in fluorine chemical potential at the two electrodes.

The apparatus used in this study for measurement of electromotive force (emf) was almost identical to that described earlier.[7] Only a brief account is given here. The electrode pellets were spring loaded on either side of transparent single crystal CaF_2 electrolyte with a gold mesh sandwiched between each electrode pellet and the electrolyte. Gold electrical leads were spot-welded to the mesh. The presence of the gold catalyst at the electrolyte-electrode interface was found necessary to obtain reproducible emf. Without the catalyst, the emf of the cell was found to be lower than the equilibrium value, especially at lower temperatures, and the response significantly slower. The pellets were held together under pressure by a system of alumina tubes and rods. Au foils were placed to prevent physical contact between the electrode pellets and alumina rods and tubes used for holding the pellets under pressure. The cell was enclosed in an outer impervious alumina tube, closed at both ends with brass caps, which had provision for gas inlet and outlet, and electrode and thermocouple leads. The alumina tube was suspended in a vertical resistance furnace. The cell was situated in the even-temperature zone (±1 K) of the furnace. A Faraday cage made of stainless steel foil was placed between the alumina tube and the furnace. The foil was earthed to minimize induced emf on cell leads from furnace winding.

After assembling the cell and raising its temperature to 573 K under flowing oxygen gas, the outer alumina tube enclosing the cell was evacuated and then refilled with oxygen gas. The procedure was repeated three times to remove moisture that desorbed from the ceramic tubes. The cell was then operated under pre-purified oxygen gas flowing at a rate of 3 mL s^{-1}. The same gas flowed over both electrodes. The cell emf was measured as a function of temperature using a high-impedance ($>10^{12}$ Ω) digital voltmeter with a sensitivity of ±0.01 mV. The emf of the cell was independent (±0.2 mV) of the flow rate of the gas in the range 1.5-5 mL s^{-1} and was reproducible on temperature cycling. The temperature of the cell was measured with a Pt/Pt-13%Rh thermocouple checked against the melting temperature of gold.

The emf became steady in 30-50 ks after the attainment of thermal equilibrium, depending on the temperature of the cell. The reversibility of the cell at different temperatures was checked by microcoulometric titration (~3 μA for 150 s) in both directions using an external potential source. In each case, the cell emf returned to its original value before the titration within 3 ks. This demonstrated that the chemical potential of fluorine at the electrodes returned to the same value after essentially infinitesimal displacements from equilibrium to both lower and higher values. To check for the presence of any thermal gradient across the cell and other stray contributions to the emf, the open circuit potential of a symmetric cell with identical electrodes

$$Au,\ O_2,\ CaO + CaF_2/CaF_2/CaF_2 + CaO,\ O_2,\ Au \quad \text{(Eq 2)}$$

was measured as a function of temperature. The emf was found to lie in a narrow range, (±0.16 mV), without any systematic trends.

Thermodynamic data[8] indicate that CaF_2 is stable in contact with CaO and TiO_2 in dry oxygen. At the end of each experiment, the cell was cooled and the electrodes were examined by optical and scanning electron microscopy, and XRD. No change in the phase composition of the electrodes during electrochemical measurement was detected. The composition of different phases present in the electrodes was checked by energy dispersive analysis of x-rays (EDX). There was no significant solid solubility either between the oxides, or between oxides and CaF_2 present at the electrodes. There was no evidence of reaction between CaF_2 single crystal and the electrode pellets at temperatures up to 1250 K. The most important factor for successful operation of the electrochemical cell was the removal of trace amounts of CO_2 and H_2O from the gas phase. Reaction of CaF_2 electrolyte with moisture resulted in an opaque coating of CaO on the electrolyte surface and deterioration in the performance of the cell.

3. Results and Discussion

The reversible emf of cell is displayed in Fig. 3 as a function of temperature. At 900 K, the cell emf was monitored for periods up to 120 ks after registering a constant value. The emf remained constant during this entire period. Within experimental uncertainty, the emf can be expressed as a linear function of temperature

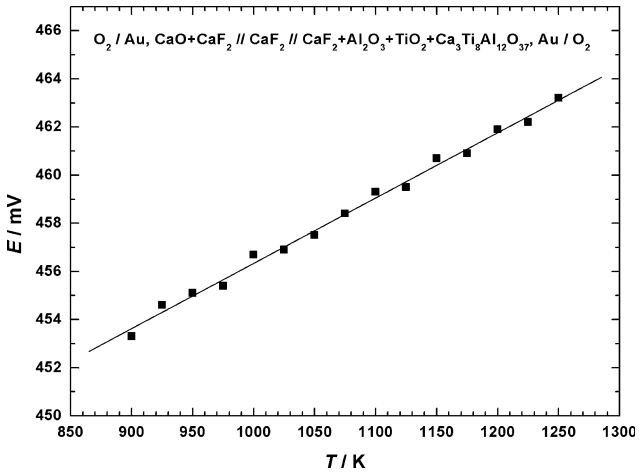

Fig. 3 Temperature dependence of the reversible emf of solid state cell I (■)

$$E(\pm 0.12)/\text{mV} = 429.21 + 0.02713(T/\text{K}). \quad \text{(Eq 3)}$$

The CaF_2 + CaO mixture converts the oxygen chemical potential of the gas phase into an equivalent fluorine chemical potential at the electrode/electrolyte interface. The analogous use of CaF_2 + CaS, CaF_2 + CaN, and CaF_2 + $CaSO_4$ couples to convert chemical potentials of S_2, N_2, and SO_3 (SO_2 + O_2) to corresponding fluorine potentials have been demonstrated earlier.[9-11] The electrochemical reaction at the measuring electrode on the right-hand side of cell is

$$3CaF_2 + 3/2O_2 + 6Al_2O_3 + 8TiO_2 + 6e^- \rightarrow Ca_3Ti_8Al_{12}O_{37} + 6F^-. \quad \text{(Eq 4)}$$

At the reference electrode on the left-hand side of the cell, the electrochemical reaction is

$$3CaO + 6F^- \rightarrow 3CaF_2 + 3/2O_2 + 6e^-. \quad \text{(Eq 5)}$$

Since oxygen partial pressure is the same over both the electrodes, the net cell reaction is the formation of the quaternary oxide from its component binary oxides according to the reaction:

$$3CaO + 6Al_2O_3 + 8TiO_2 \rightarrow Ca_3Ti_8Al_{12}O_{37}. \quad \text{(Eq 6)}$$

Throughout this paper the reference state for solid TiO_2 is the rutile form and for Al_2O_3 the α form. CaF_2 is a fluorine ion conductor, with ionic transport number greater than 0.99, at the temperatures and fluorine chemical potentials encountered in this study.[12,13] Since there was no significant solid solubility between CaF_2, CaO, TiO_2, and $Ca_3Ti_8Al_{12}O_{37}$ at the temperatures covered in this study, the compounds are present at unit activity at the electrodes. The standard Gibbs free energy change associated with the cell reaction is directly related to the emf by the Nernst equation;

$$\Delta G^{\circ}_{r(6)}(\pm 70)/\text{J mol}^{-1} = -6FE = -248474 - 15.706(T/\text{K}) \quad \text{(Eq 7)}$$

where $\Delta G^{\circ}_{r(6)}$ is the standard Gibbs free energy change for reaction (6) and F is the Faraday constant. The temperature-independent term on the right hand side of Eq 7 gives the enthalpy of formation of $Ca_3Ti_8Al_{12}O_{37}$ from component binary oxides at an average temperature of 1075 K. The temperature dependent term is related to the corresponding entropy of formation. The small positive entropy of formation makes the Gibbs free energy of formation marginally more negative with increasing temperature. Invoking the Neumann Kopp rule to estimate the heat capacity of $Ca_3Ti_8Al_{12}O_{37}$ relative to those of its component oxides, enthalpy of formation of $Ca_3Ti_8Al_{12}O_{37}$ from elements at 298.15 K can be evaluated as −19765.92 (±13) kJ mol^{-1}. Similarly, the standard entropy of $Ca_3Ti_8Al_{12}O_{37}$ at 298.15 K can be estimated as 838.38(±2) J mol^{-1} K^{-1}. The auxiliary data for enthalpy of formation and the entropy of Al_2O_3, TiO_2, and CaO are taken form NIST-JANAF tables.[8]

The cell reaction can also be formulated as the transfer of one mole of CaO at unit activity (standard state) on the left-hand side of the cell to CaO at reduced activity corresponding to a monovariant mixture of phases on the right-hand side of the cell. Viewed from this perspective, the cell emf is related to the difference in the chemical potential of CaO at the two electrodes:$\mu_{CaO} - \mu^{\circ}_{CaO} = -2FE$. Thus, the relative chemical potential of CaO in the three-phase field containing Al_2O_3, TiO_2, and $Ca_3Ti_8Al_{12}O_{37}$ is;

$$\Delta\mu_{CaO}(\pm 23)/\text{J mol}^{-1} = -82825 - 5.235(T/\text{K}). \quad \text{(Eq 8)}$$

4. Phase Diagrams for the System Al_2O_3-CaO-TiO_2

Based on thermodynamic data for $Ca_3Ti_8Al_{12}O_{37}$ determined in this study and data for calcium titanates and aluminates reported earlier[7,14] and summarized in Table 2, subsolidus phase relations in the system Al_2O_3-TiO_2-CaO can be computed using the free energy minimization procedure. The isothermal section of the phase diagram at 1200 K is shown in Fig. 4.

There is controversy regarding stability of the compound $Ca_{12}Al_{14}O_{33}$ along the binary Al_2O_3-CaO. One school of thought considers the phase to be stabilized by moisture or halogens; it is not strictly a stable phase in the binary Al_2O_3-CaO system.[15] The other school considers it as a stable phase in the binary based on thermodynamic and phase equilibrium data.[14,16,17] Cockayne and Lent[18] have grown single crystals of $Ca_{12}Al_{14}O_{33}$ several centimeters long from melt. Although a small infrared absorption band at 2.8 μm corresponding to hydroxyl ions was observed, the intensity was unaffected by prolonged vacuum treatment, suggesting that the hydroxyl ion was present as a minor impurity rather than as a constituent. In the system Ca-Al-O, liquid Al-Ca alloys were found to be in equilibrium with $Ca_{12}Al_{14}O_{33}$ at 1373 K.[19] The experimental data for alloy-oxide equilibrium was in reasonable agreement with thermodynamic calculations. The interoxide phase was also identified as product during the reduction of CaO by Al under vacuum.[20,21] Since hydroxyl ions would not be stable in the

Table 2 Gibbs free energies of formation of ternary and quaternary compounds from component binary oxides CaO, Al_2O_3, and TiO_2

No.	Compound	Free energy, kJ mol^{-1}	Temperature range, K	References
1	$CaA_{l2}O_{19}$	$-17430 - 37.2T$ (±1500)	923-1900	[14]
2	$CaAl_4O_7$	$-16400 - 26.8T$ (±2500)	923-1900	[14]
3	$CaAl_2O_4$	$-18120 - 18.62T$ (±1500)	923-1900	[14]
4	$Ca_{12}Al_{14}O_{33}$	$-86100 - 205.1T$ (±17500)	923-1600	[14]
5	$Ca_3Al_2O_6$	$-17000 - 32.0T$ (±1500)	923-1800	[14]
6	$Ca_3Ti_2O_7$	$-164217 - 16.838T$ (±185)	900-1250	[7]
7	$Ca_4Ti_3O_{10}$	$-243473 - 25.758T$ (±275)	900-1250	[7]
8	$CaTiO_3$	$-80140 - 6.302T$ (±85)	900-1250	[7]
9	$Ca_3Ti_8Al_{12}O_{37}$	$-248474 - 15.706T$ (±70)	900-1250	This study

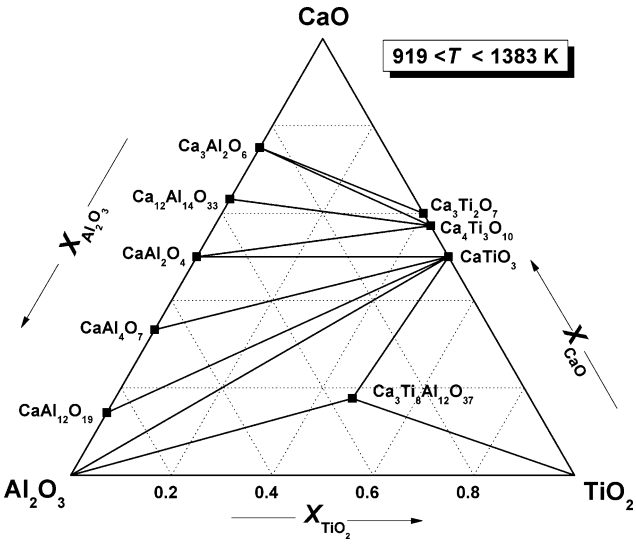

Fig. 4 The isothermal section of the phase diagram of the system Al_2O_3-TiO_2-CaO calculated at 1200 K. The diagram is valid in the temperature range from 919 to 1383 K

presence of Ca vapor, these results suggest that $Ca_{12}Al_{14}O_{33}$ is stable even in the absence of moisture. The structure of $Ca_{12}Al_{14}O_{33}$ is composed of a positively charged lattice framework, $[Ca_{24}Al_{48}O_{64}]^{4+}$, with 12 subnanometer-sized cages in a cubic unit cell. To maintain charge neutrality, additional O^{2-} ions randomly occupy two of these 12 cages.[22] Various anions (F^-, Cl^-, OH^-, O^-, and O_2^-) can replace O^{2-} ions in the cage.[23-26] Recent results indicate that a part of the O^{2-} ions in the cage can be removed under reducing conditions (carbon container) at high temperatures producing a nonstoichiometric oxide with high electronic conductivity.[27] The XRD pattern of $Ca_{12}Al_{14}O_{33}$ exposed to reducing conditions was almost identical to that of the sample heated in dry oxygen. In the light of the above evidence, $Ca_{12}Al_{14}O_{33}$ is retained as a stable phase in all diagrams in this paper above 919 K.

The correct phase diagram must satisfy some thermodynamic requirements for internal consistency.[28] The chemical potentials of the apex component (such as CaO) should increase when different phase fields are traversed along any line joining a composition on the opposite binary (Al_2O_3-TiO_2 in this example) to the apex (Kohler isogram; $X_{Al_2O_3}/X_{TiO_2}$ = constant). Figure 5 shows the relative chemical potential of CaO as a function of temperature for various phase fields depicted in Fig. 4. When two adjacent oxide phases along either of the binaries CaO-Al_2O_3 and CaO-TiO_2 coexist with a third phase, the chemical potential of CaO is determined by the thermodynamic properties of the two compounds along the binary.[28] Figure 5 shows that the thermodynamic requirement for increasing chemical potential is clearly satisfied at 1200 K and over a large temperature interval from 919 to 1383 K. Thus, Fig. 4 would be valid in this temperature range. Minor changes in isothermal section will occur below and above this temperature range, since the line corresponding to chemical potential of the phase mixture $CaAl_2O_4$ + $Ca_{12}Al_{14}O_{33}$ cuts the lines corresponding to $Ca_{12}Al_{14}O_{33}$ + $Ca_3Al_2O_6$, and $CaTiO_3$ + $Ca_4Ti_3O_{10}$ at 919 and 1383 K, respectively. Isothermal sections for $T < 919$ K and above $T > 1383$ K are shown in Fig. 6 and 7. At the lower temperatures the equilibrium phase mixtures may not be realized even over extended periods because of kinetic restrictions.

Increasing temperature above 1496 K results in the formation of Al_2TiO_5 along the binary Al_2O_3-TiO_2. Independent studies[29] indicate that the standard Gibbs energy of formation of Al_2TiO_5 from component oxides can be expressed as;

$$Al_2O_3 + TiO_2 \rightarrow Al_2TiO_5 \qquad \text{(Eq 9)}$$

$$\Delta G^{o}_{r(9)}/\mathrm{J\,mol^{-1}} = 3742 - 2.501(T/K). \qquad \text{(Eq 10)}$$

Consequent to the formation of Al_2TiO_5, the stability of $Ca_3Ti_8Al_{12}O_{37}$ must be reassessed in relation to its immediate neighbors. For the reaction

$$3CaTiO_3 + 5Al_2TiO_5 + Al_2O_3 \rightarrow Ca_3Ti_8Al_{12}O_{37} \qquad \text{(Eq 11)}$$

$$\Delta G^{o}_{r(11)}/\mathrm{J\,mol^{-1}} = -26764 + 15.705(T/K). \qquad \text{(Eq 12)}$$

Free energy change for reaction (11) becomes zero at $T = 1704$ K. Therefore the quaternary oxide becomes unstable at $T > 1704$ K. The corresponding isothermal sections of the phase diagrams for $1496 < T < 1704$ K and $T > 1704$ K are shown in Fig. 8 and 9. Morgan and

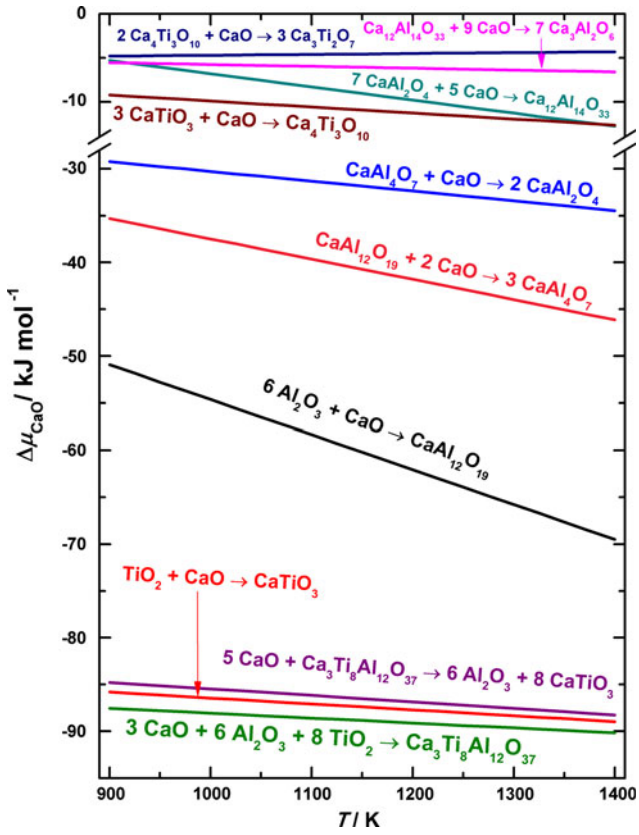

Fig. 5 The relative chemical potential of CaO as a function of temperature for various phase fields depicted in Fig. 3

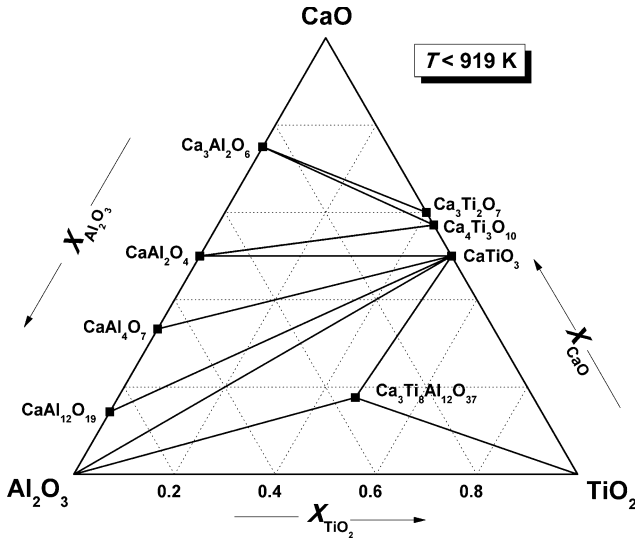

Fig. 6 The isothermal section of the phase diagram of the system Al_2O_3-TiO_2-CaO at $T < 919$ K

Koutsoutis[3] report the upper stability limit of $CaTi_3Al_8O_{19}$ (identified as $Ca_3Ti_8Al_{12}O_{37}$ in this study) as 1693(±50) K. Thus the availability of new thermodynamic information on $Ca_3Ti_8Al_{12}O_{37}$ has enabled the construction of the phase diagram for the system Al_2O_3-CaO-TiO_2 as a function of temperature.

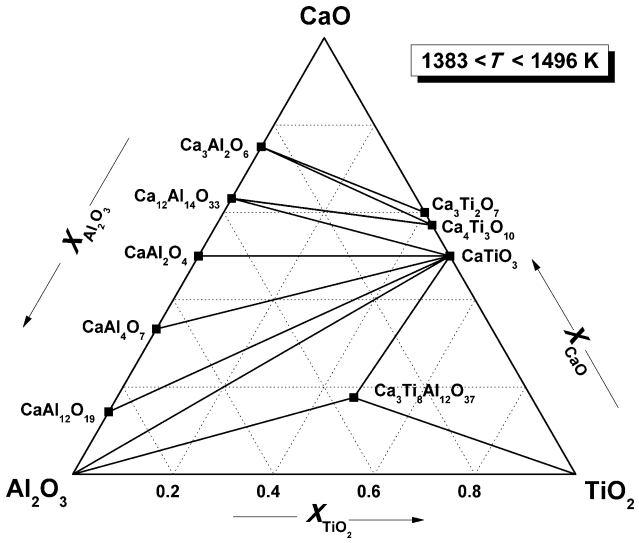

Fig. 7 The isothermal section of the phase diagram of the system Al_2O_3-TiO_2-CaO at $1383 < T < 1496$ K

5. Chemical Potential Diagrams

The stability domain of different phases at constant temperature and total pressure can be depicted in two dimensions by plotting the chemical potential of one of the components of the pseudo-ternary system as a function of the normalized mole fraction of the other two components. The composition of a component is normally designated by its mole fraction, which is obtained by dividing the number of moles of the component with the sum of moles of all components. The normalized mole fraction, used as the composition variable in chemical-potential diagrams, is obtained by removing the component, the chemical potential of which is being plotted, from the summation in the denominator. Thus, the chemical potential becomes an independent variable with respect to the normalized mole fraction.

The variation of the chemical potentials of CaO, Al_2O_3, and TiO_2 with the corresponding normalized mole fractions in the Al_2O_3-TiO_2-CaO system at 1200 K and standard pressure are shown in the Fig. 10, 11, and 12. The diagrams are calculated using the Gibbs energy of formation of the quaternary phase ($Ca_3Ti_8Al_{12}O_{37}$) determined in the present study, and standard Gibbs energies of formation of calcium titanates ($Ca_3Ti_2O_7$, $Ca_4Ti_3O_{10}$, and $CaTiO_3$) and calcium aluminates ($CaAl_{12}O_{19}$, $CaAl_4O_7$, $CaAl_2O_4$, $Ca_{12}Al_{14}O_{33}$, and $Ca_3Al_2O_6$) from the literature.[7,14] The data used for calculations are summarized in Table 2. When three condensed phases coexist at constant temperature and pressure, the chemical potential is invariant and can be represented by a horizontal line on the diagrams. The diagrams obey the same topological rules of construction that are applicable to the more familiar temperature-composition (*T*-*X*) phase diagrams. The chemical potential diagrams provide complementary information regarding phase equilibria which are conventionally represented on the Gibbs ternary triangle (Fig. 4). The diagrams show the

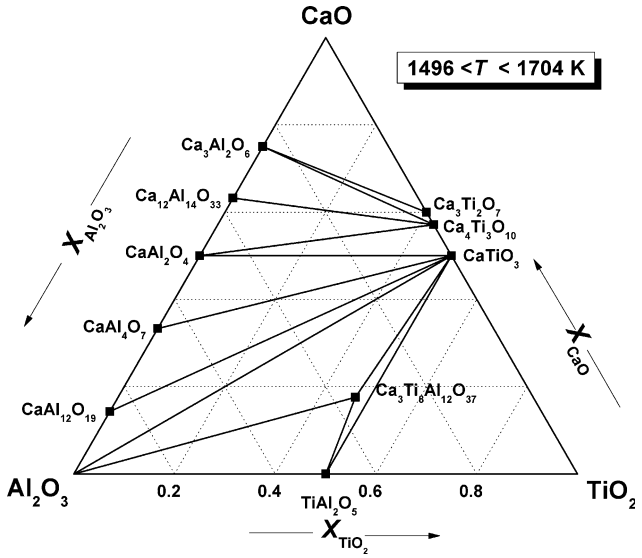

Fig. 8 The isothermal section of the phase diagram of the system Al_2O_3-TiO_2-CaO at $1496 < T < 1704$ K

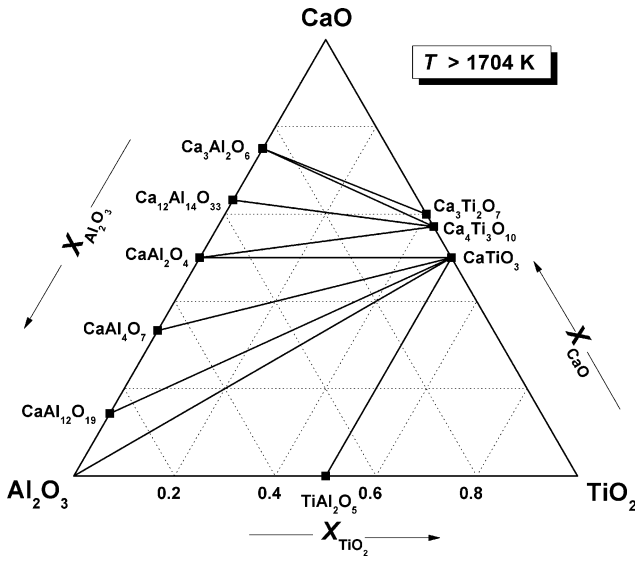

Fig. 9 Subsolidus phase relations in the system Al_2O_3-TiO_2-CaO at $T > 1704$ K

variation of the chemical potential of an apex species as one proceeds from the binary system represented by a side of the ternary triangle towards the opposite apex.

Presented in Fig. 10 is the variation of the chemical potential of CaO with the normalized mole fraction $\eta_{Ti}/(\eta_{Ti} + \eta_{Al})$ at 1200 K. The diagram displays the chemical potential range for the stability of various phases. The reactions that define the chemical potential of CaO are listed in Table 3. Three-phase equilibria are represented by horizontal lines connecting the compositions of the three phases. Only two-phase fields are labeled on the diagram. The two-phase field containing Al_2O_3 and $CaTiO_3$ extends over a large range of chemical potential; a break is inserted in the *y*-axis in this phase field to magnify the other regions.

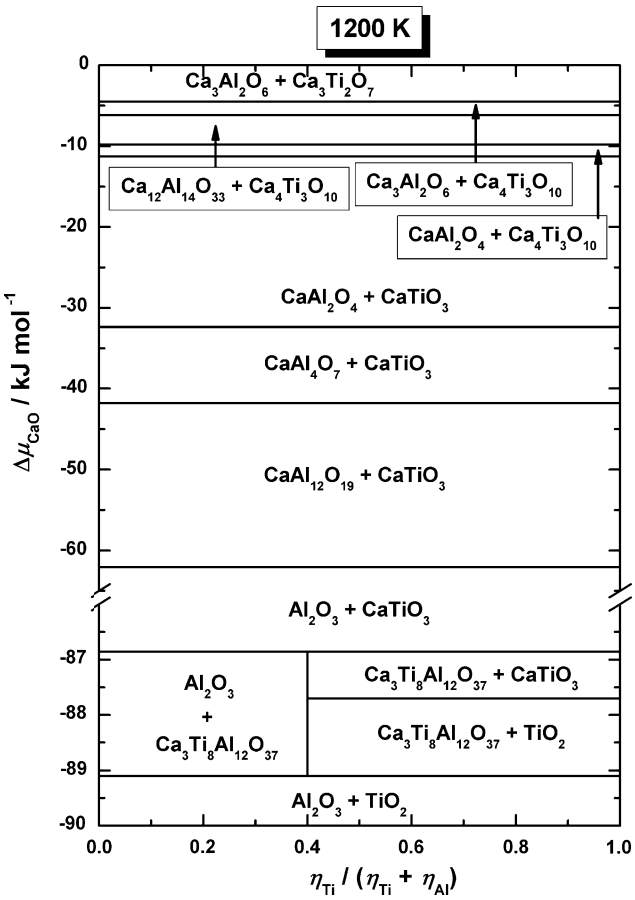

Fig. 10 The variation of the chemical potentials of CaO with the corresponding normalized mole fraction in the Al_2O_3-TiO_2-CaO system at 1200 K and standard pressure

It is seen from the diagram that the quaternary oxide $Ca_3Ti_8Al_{12}O_{37}$ is stable only in a narrow range of chemical potential at the lower part of the diagram.

The variation of the chemical potential of Al_2O_3 with the normalized mole fraction, $\eta_{Ti}/(\eta_{Ti} + \eta_{Ca})$, in the ternary system Al_2O_3-TiO_2-CaO at 1200 K is shown in the Fig. 11. The standard state for Al_2O_3 is the α form. The reactions defining the chemical potential of Al_2O_3 are summarized in Table 4. The quaternary oxide $Ca_3Ti_8Al_{12}O_{37}$ is stable only in a narrow range of chemical potential in the upper part of the diagram.

The variation of the chemical potential of TiO_2 with the normalized mole fraction, $\eta_{Al}/(\eta_{Al} + \eta_{Ca})$, in the ternary system Al_2O_3-TiO_2-CaO at 1200 K is shown in the Fig. 12. The standard state for TiO_2 is the rutile form. The reactions defining the chemical potential of TiO_2 are summarized in Table 5. The quaternary oxide $Ca_3Ti_8Al_{12}O_{37}$ is stable only in a narrow range of chemical potential in the upper part of the diagram.

6. Conclusions

The standard Gibbs energy of formation of $Ca_3Ti_8Al_{12}O_{37}$ from component binary oxides has been measured

accurately in the temperature range from 900 to 1250 K using a solid-state electrochemical cell incorporating single crystal CaF_2 as the solid electrolyte. For the reaction,

$$3CaO + 6Al_2O_3 + 8TiO_2 \rightarrow Ca_3Ti_8Al_{12}O_{37}$$

$$\Delta G^{o}_{f(ox)}(\pm 70)/J\,mol^{-1} = -248474 - 15.706(T/K).$$

Combining the high-temperature results with Neumann Koop rule and auxiliary data on Al_2O_3, TiO_2, and CaO form NIST-JANAF tables, thermodynamic properties of $Ca_3Ti_8Al_{12}O_{37}$ at 298.15 K are evaluated: $\Delta H^{o}_{f(298.15\,K)} = -19765.92(\pm 13)\,kJ\,mol^{-1}$ and $S^{o}_{298.15\,K} = 838.38(\pm 2)\,J\,mol^{-1}\,K^{-1}$. The results obtained in this study provide the only information now available for this compound.

Using the data for $Ca_3Ti_8Al_{12}O_{37}$ obtained in this study along with data for other aluminate and titanate phases

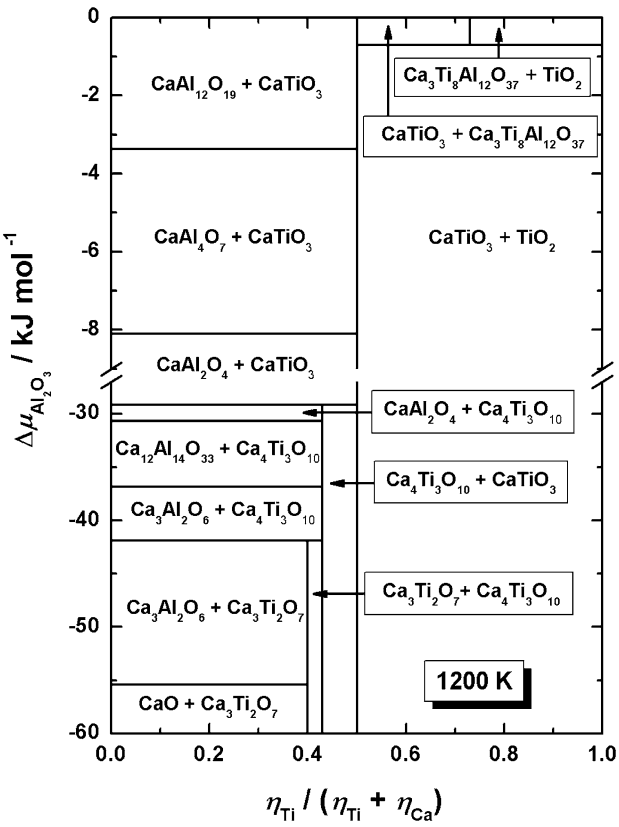

Fig. 11 The variation of the chemical potentials of Al_2O_3 with the corresponding normalized mole fraction in the Al_2O_3-TiO_2-CaO system at 1200 K and standard pressure

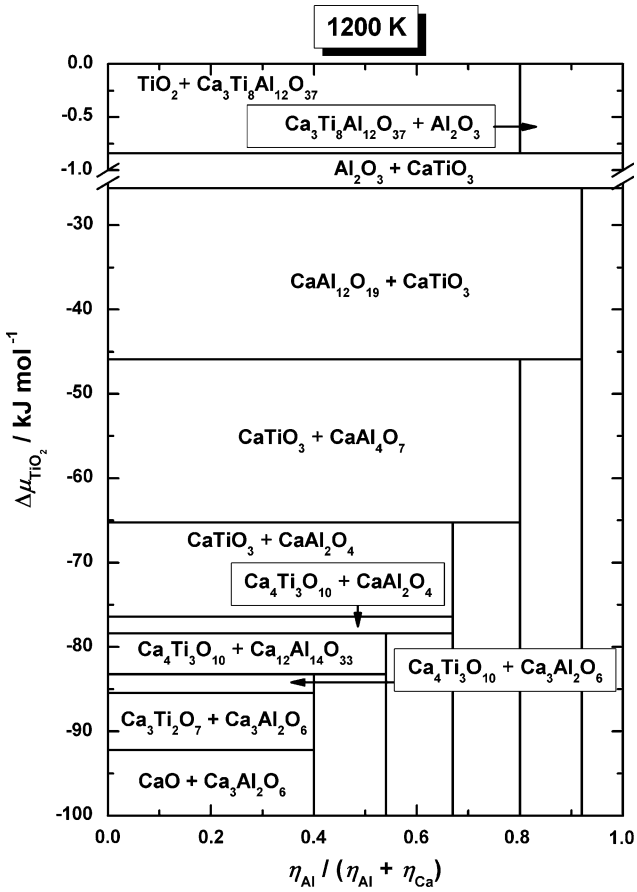

Fig. 12 The variation of the chemical potentials of TiO_2 with the corresponding normalized mole fraction in the Al_2O_3-TiO_2-CaO system at 1200 K and standard pressure

Table 3 Reactions and corresponding chemical potentials of CaO at 1200 K in the system Al_2O_3-TiO_2-CaO

No.	Reactions defining $\Delta\mu_{CaO}$	Composition of phases $\eta_{Ti}/(\eta_{Ti} + \eta_{Al})$	$\Delta\mu_{CaO}$, kJ mol^{-1}
1	$6Al_2O_3 + 8TiO_2 + 3CaO \rightarrow Ca_3Ti_8Al_{12}O_{37}$	0, 1, 0.4	−89.107
2	$TiO_2 + CaO \rightarrow CaTiO_3$	1, 1	−87.702
3	$Ca_3Ti_8Al_{12}O_{37} + 5CaO \rightarrow 8CaTiO_3 + 6Al_2O_3$	0.4, 1, 0	−86.859
4	$6Al_2O_3 + CaO \rightarrow CaAl_{12}O_{19}$	0, 0	−62.070
5	$CaAl_{12}O_{19} + 2CaO \rightarrow 3CaAl_4O_7$	0, 0	−41.805
6	$CaAl_4O_7 + CaO \rightarrow 2CaAl_2O_4$	0, 0	−32.368
7	$3CaTiO_3 + CaO \rightarrow Ca_4Ti_3O_{10}$	1, 1	−11.275
8	$7CaAl_2O_4 + 5CaO \rightarrow Ca_{12}Al_{14}O_{33}$	0, 0	−9.794
9	$Ca_{12}Al_{14}O_{33} + 9CaO \rightarrow 7Ca_3Al_2O_6$	0, 0	−6.176
10	$2Ca_4Ti_3O_{10} + CaO \rightarrow 3Ca_3Ti_2O_7$	1, 1	−4.504

Table 4 Reactions and corresponding chemical potentials of Al_2O_3 at 1200 K in the system Al_2O_3-TiO_2-CaO

No.	Reactions defining $\Delta\mu_{Al_2O_3}$	Composition of phases $\eta_{Ti}/(\eta_{Ti}+\eta_{Ca})$	$\Delta\mu_{Al_2O_3}$, kJ mol^{-1}
1	$3CaO + Al_2O_3 \rightarrow Ca_3Al_2O_6$	0, 0	−55.400
2	$9Ca_3Ti_2O_7 + Al_2O_3 \rightarrow 6Ca_4Ti_3O_{10} + Ca_3Al_2O_6$	0.4, 0.43, 0	−41.892
3	$4Ca_3Al_2O_6 + 3Al_2O_3 \rightarrow Ca_{12}Al_{14}O_{33}$	0, 0	−36.873
4	$Ca_{12}Al_{14}O_{33} + 5Al_2O_3 \rightarrow 12CaAl_2O_4$	0, 0	−30.670
5	$Ca_4Ti_3O_{10} + Al_2O_3 \rightarrow 3CaTiO_3 + CaAl_2O_4$	0.43, 0.5, 0	−29.189
6	$CaAl_2O_4 + Al_2O_3 \rightarrow CaAl_4O_7$	0, 0	−8.096
7	$CaAl_4O_7 + 4Al_2O_3 \rightarrow CaAl_{l2}O_{19}$	0, 0	−3.378
8	$3CaTiO_3 + 6Al_2O_3 + 5TiO_2 \rightarrow Ca_3Ti_8Al_{12}O_{37}$	0.5, 1, 0.73	−0.702

Table 5 Reactions and corresponding chemical potentials of TiO_2 at 1200 K in the system Al_2O_3-TiO_2-CaO

No.	Reactions defining $\Delta\mu_{TiO_2}$	Composition of phases $\eta_{Al}/(\eta_{Al}+\eta_{Ca})$	$\Delta\mu_{TiO_2}$, kJ mol^{-1}
1	$3CaO + 2TiO_2 \rightarrow Ca_3Ti_2O_7$	0, 0	−92.211
2	$4Ca_3Ti_2O_7 + TiO_2 \rightarrow 3Ca_4Ti_3O_{10}$	0, 0	−85.457
3	$28Ca_3Al_2O_6 + 27TiO_2 \rightarrow 9Ca_4Ti_3O_{10} + 4Ca_{12}Al_{14}O_{33}$	0.4, 0, 0.54	−83.227
4	$4Ca_{12}Al_{14}O_{33} + 15TiO_2 \rightarrow 5Ca_4Ti_3O_{10} + 28CaAl_2O_4$	0.54, 0, 0.67	−78.402
5	$Ca_4Ti_3O_{10} + TiO_2 \rightarrow 4CaTiO_3$	0, 0	−76.427
6	$2CaAl_2O_4 + TiO_2 \rightarrow CaTiO_3 + CaAl_4O_7$	0.67, 0, 0.8	−65.266
7	$3CaAl_4O_7 + 2TiO_2 \rightarrow 2CaTiO_3 + CaAl_{l2}O_{19}$	0.8, 0, 0.92	−45.897
8	$CaAl_{l2}O_{19} + TiO_2 \rightarrow CaTiO_3 + 6Al_2O_3$	0.92, 0, 1	−25.632
9	$3CaTiO_3 + 6Al_2O_3 + 5TiO_2 \rightarrow Ca_3Ti_8Al_{12}O_{37}$	0, 1, 0.8	−0.843

published earlier, subsolidus phase relations have been developed as a function of temperature for the pseudo-ternary system Al_2O_3-CaO-TiO_2 at high oxygen potentials. The isothermal sections computed in this study supersede those given in the phase diagram compilations of the American Ceramic Society. Chemical potential diagrams are computed at 1200 K, showing the stability domains of the various phases in the chemical potential-composition space.

Acknowledgments

This work was partially supported by the University Grants Commission, India, through the award of Dr. D.S. Kothari Postdoctoral Fellowship to G. Rajitha, and by the Indian National Academy of Engineering through the award of Distinguished Professorship to K.T. Jacob.

References

1. P.E.D. Morgan, Preparing New Extremely Difficult-to-Form Crystal Structures, *Mater. Res. Bull.*, 1984, **19**(3), p 369-376
2. H.W. Zandbergen and D.J.W. Ijdo, New Compounds in the System SrO-TiO_2-Al_2O_3 at 1300 °C a Crystallographic and Leaching Study, *Mater. Res. Bull.*, 1983, **18**(3), p 371-374
3. P.E.D. Morgan and M.S. Koutsoutis, Phase Relations in the Ca-Ti-Al-O System; Further Studies on Members of the CTA Family, *J. Mater. Sci. Lett.*, 1985, **4**(3), p 321-323
4. Fig. 10049, *Phase Diagrams for Ceramists*, Vol. XII, H.F. McMurdie, and R.S. Roth, Ed., The American Ceramic Society, Westerville, 1996
5. Fig. EC-466, *Phase Diagrams for Electronic Ceramics I*, R.S. Roth, Ed., The American Ceramic Society, Westerville, 2003
6. K.T. Jacob, K.P. Jayadevan, R.M. Mallya, and Y. Waseda, Nanocrystalline $MgAl_2O_4$: Measurement of Thermodynamic Properties Using a Solid State Cell, *Adv. Mater.*, 2000, **12**(6), p 440-444
7. K.T. Jacob and K.P. Abraham, Thermodynamic Properties of Calcium Titanates: $CaTiO_3$, $Ca_4Ti_3O_{10}$, and $Ca_3Ti_2O_7$, *J. Chem. Thermodyn.*, 2009, **41**(6), p 816-820
8. M.W. Chase, Jr., Journal of Physical and Chemical Reference Data, Monograph No. 9, *NIST-JANAF Thermochemical Tables,* 4th ed., 1998, p 716
9. K.T. Jacob, D.B. Rao, and H.G. Nelson, Some Studies on a Solid-State Sulfur Probe for Coal Gasification Systems, *J. Electrochem. Soc.*, 1978, **125**(5), p 758-762
10. K.T. Jacob, S. Singh, and Y. Waseda, Refinement of Thermodynamic Data on GaN, *J. Mater. Res.*, 2007, **22**(12), p 3475-3483
11. K.T. Jacob, M. Iwase, and Y. Waseda, A Galvanic Sensor for SO_3/SO_2 Based on the $CaF_2/CaSO_4$ Couple, *Solid State Ion.*, 1987, **23**(4), p 245-252
12. J. Delcet, R.J. Heus, and J.J. Egan, Electronic Conductivity in Solid CaF_2 at High Temperature, *J. Electrochem. Soc.*, 1978, **125**(5), p 755-758
13. K. Ono, T. Fujimura, and J. Moriyama, Conductivity Measurements of CaF_2 Crystal under Controlled Fluorine Chemical Potentials, *J. Jpn. Inst. Met.*, 1978, **42**(5), p 469-474
14. M. Allibert, C. Chatillon, K.T. Jacob, and R. Lourtau, Mass-Spectrometric and Electrochemical Studies of Thermodynamic

Properties of Liquid and Solid Phases in the System CaO-Al_2O_3, *J. Am. Ceram. Soc.*, 1981, **64**(5), p 307-314
15. R.W. Nurse, J.H. Welch, and A.J. Majumdar, The CaO-Al_2O_3 System in a Moisture-Free Atmosphere, *Trans. Br. Ceram. Soc.*, 1965, **64**(9), p 409-418
16. R.G.J. Ball, M.A. Mignanelli, T.I. Barry, and J.A. Gisby, The Calculation of Phase Equilibria of Oxide Core-Concrete Systems, *J. Nucl. Mater.*, 1993, **201**, p 238-249
17. A.K. Chatterjee and G.I. Zhmoidin, The Phase Equilibrium Diagram of the System CaO-Al_2O_3-CaF_2, *J. Mater. Sci.*, 1972, **7**(1), p 93-97
18. B. Cockayne and B. Lent, Single Crystal Growth of 12CaO-$7Al_2O_3$, *J. Cryst. Growth*, 1979, **46**(4), p 467-473
19. S. Srikanth, V.S. Srinivasan, K.T. Jacob, and M. Allibert, Alloy-Oxide Equilibria in the System Ca-Al-O at 1373 K, *Rev. Int. Hautes. Temp. Refract.*, 1991, **27**(3), p 131-139
20. S. Srikanth and K.T. Jacob, Vapour Pressure of Calcium Corresponding to the Reduction of Calcia by Aluminium, *Trans. Indian Inst. Met.*, 1991, **44**(5), p 369-373
21. K.T. Jacob and S. Srikanth, Physical Chemistry of the Reduction of Calcium Oxide with Aluminium in Vacuum, *High Temp. Mater. Process. (Lond.)*, 1990, **9**(2-4), p 77-92
22. H.B. Bartl and T. Scheller, Zur Struktur Des 12CaO·$7Al_2O_3$, *N. Jb. Miner. Mh.*, 1970, **35**, p 547-552, in German
23. J. Jeevaratnam, F.P. Glasser, and L.S.D. Glasser, Anion Substitution and Structure of 12CaO·7A1_2O_3, *J. Am. Ceram. Soc.*, 1964, **47**(2), p 105-106
24. J.A. Imlach, L.S. Dent Glasser, and F.P. Glasser, Excess Oxygen and the Stability of "12CaO·$7A_2O_3$", *Cem. Concr. Res.*, 1971, **1**(1), p 57-61
25. H. Hosono and Y. Abe, Occurrence of Superoxide Radical Ion in Crystalline 12CaO·$7Al_2O_3$ Prepared Via Solid-State Reactions, *Inorg. Chem.*, 1987, **26**(8), p 1192-1195
26. K. Hayashi, M. Hirano, S. Matsuishi, and H. Hosono, Microporous Crystal 12CaO·$7Al_2O_3$ Encaging Abundant O^- Radicals, *J. Am. Chem. Soc.*, 2002, **124**(5), p 738-739
27. S.W. Kim, K. Hayashi, M. Hirano, H. Hosono, and I. Tanaka, Electron Carrier Generation in a Refractory Oxide 12CaO·7A-l_2O_3 by Heating in Reducing Atmosphere: Conversion from an Insulator to a Persistent Conductor, *J. Am. Ceram. Soc.*, 2006, **89**(10), p 3294-3298
28. S.V. Varamban and K.T. Jacob, Thermodynamic Constraints Along Isograms in Ternary Systems: Application to Three-Phase Equilibria, *Mater. Sci. Eng. B*, 1997, **49**(2), p 100-109
29. K.T. Jacob, Unpublished work